$Me_3TTF-PO_3H_2$, a Redox Phosphonic Acid and its Monoanilinium Salt $[PhNH_3^+][Me_3TTF-PO(OH)O^-]$, the Electrocrystallized Neutral (Zwitterionic) π Radical $[Me_3TTF-PO(OH)O^-]^{\cdot+}$, and Their Associated Lamellar Constructions in the Solid State

Anne Dolbecq, Marc Fourmigué, Frederik C. Krebs, Patrick Batail,* Enric Canadell,* Rodolphe Clérac, and Claude Coulon

Abstract: The reaction of Me_3TTFLi (TTF = tetrathiafulvalene) with $ClP(O)(OEt)_2$ followed by hydrolysis with Me_3SiBr affords the novel π-donor molecule trimethyltetrathiafulvalenylphosphonic acid ($Me_3TTF-PO_3H_2$) in a partially oxidized form. Subsequent reduction and neutralization with aniline gives the corresponding phosphonate monoanilinium salt. A unique hydrogen-bonded hexagonal net is identified within the lamellar structure of $[PhNH_3^+][Me_3TTF-PO(OH)O^-]$, which is described by analogy with the anti-$CaSi_2$ structure type. Electrocrystallization of the former salt yields single crystals of a neutral (zwitterionic) π radical, formulated as $[Me_3TTF-PO(OH)O^-]^{\cdot+}$. Their structure reveals the presence of hydrogen-bonded molecular ribbons whose association creates a novel layered architecture similar to that obtained within radical cation salts of π-donor molecules of larger spatial extension. The analysis of the calculated HOMO–HOMO intermolecular interaction energies demonstrates that these slabs contain strong $\pi-\pi$ intermolecular interactions despite the nonexistence of any 2D network of short S···S contacts. The spin susceptibility of $[Me_3TTF-PO(OH)O^-]^{\cdot+}$, determined by single-crystal ESR measurements, is characteristic of triplet excitons, the origin of which may be understood from the electronic structure of the compound.

Keywords
crystal engineering · hydrogen bonds · phosphonates · radical cations · tetrathiafulvalenes

Introduction

The controlled construction of layered electro-,[1] photo-,[2] or catalytically[3] active molecular assemblies is the object of much present research. There are indeed great expectations in materials science if we, chemists, can devise efficient concepts that enable us to favor the aggregation of molecules into collections of two-dimensional character within bulk samples as well as thin films. The design of intermolecular hydrogen-bond patterns[4, 5] and coordination to metal ions[6] are the two major chemical tools for use in imposing directed intermolecular interactions. Note, however, that binding to one or several metal ions will in effect scale up the task by creating novel, more complex molecular objects (secondary structure). In particular, the need to control the motif of their supersecondary structure arises in turn, unless a collection of metal ions has been organized into long-range ordered mesoscale patterns prior to the binding process. Further, the ability of metal complexes of a variety of organophosphonate ligands to organize into lamellar structures has recently been well recognized and exploited.[2, 3, 7] All of these approaches have, however, so far focused on the manipulation of closed-shell molecules. Clearly, though, the energy stabilization within organized assemblies as a result of an optimized overlap of π-radical molecules has been the major guideline adopted for the synthesis of novel conducting or superconducting molecular solids and, again, there is a strong present trend in the chemistry and physics of organized radical cation solids to design highly ordered two-dimensional molecular conducting and superconducting systems.[8] We now report the series of title trimethyltetrathiafulvalene-functionalized phosphonic acid and phosphonate derivatives designed to provide precursors of a variety of layered electroactive molecular constructions, as described in this paper.

[*] Dr. P. Batail, Dr. M. Fourmigué, F. C. Krebs
Institut des Matériaux, UMR 110 CNRS–Université de Nantes
2, rue de la Houssinière, 44072 Nantes (France)
Fax: Int. code +(40)373995
Dr. A. Dolbecq
Laboratoire de Physique des Solides, Unité Associée au CNRS N° 2
Université de Paris Sud, 91405 Orsay (France)
Dr. E. Canadell
Institut de Ciencia de Materials de Barcelona (CSIC)
Campus de la UAB, 08193 Bellaterra (Spain)
and
Laboratoire de Chimie Théorique, Unité Associée au CNRS N° 506
Université de Paris Sud, 91405 Orsay (France)
Prof. C. Coulon, R. Clérac
Centre de Recherche Paul Pascal, CNRS
av. Dr. Schweitzer, 33600 Pessac (France)

Results and Discussion

Synthesis: Aromatic phosphonic acids are usually prepared by hydrolysis of the corresponding diester or diamide. Thus, Katz reported[9] the reaction of dilithiated quaterthiophene with bis-

(dimethylamino)phosphorochloridate to afford the tetraamide, easily hydrolyzed with concentrated hydrochloric acid to give the free diphosphonic acid. Because of the sensitivity of the TTF core towards both oxidative and acidic conditions, we investigated the preparation of the phosphonic acid $Me_3TTF-PO_3H_2$ under milder conditions with a stepwise reaction sequence (Scheme 1). Also, the synthesis was carried out with the

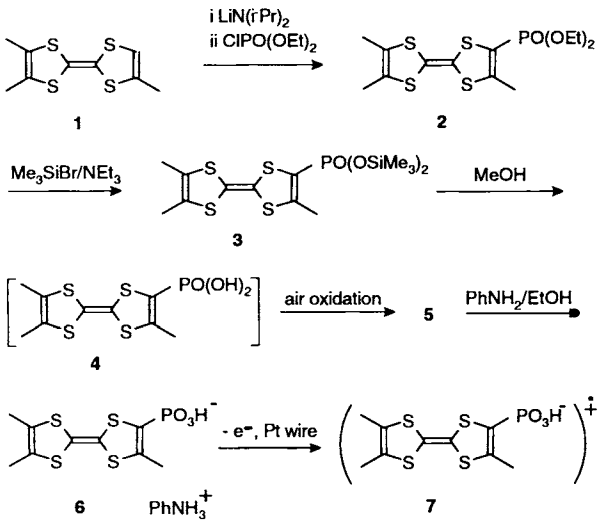

Scheme 1.

trimethyl-substituted tetrathiafulvalene core, which has been shown to yield more stable and crystalline products than the parent TTF molecule.[10] The intermediate diethyl ester **2** is prepared first from the trimethyltetrathiafulvalene **1** by lithiation[10, 11] and reaction with diethyl chlorophosphate. In the second step, **2** is converted into the bis(trimethylsilyl)ester **3** by treatment with bromotrimethylsilane and NEt_3.[12] The final hydrolysis of **3** in methanol affords a black paramagnetic powder **5** (vide infra), which is reduced with aniline to provide the monoanilinium salt of the trimethyltetrathiafulvalenylphosphonic acid, **6**. Compound **5** is insoluble in most organic solvents and dissolves slightly in water to give a green solution, a feature typical of TTF radical cations. Elemental analysis establishes the expected formulation, $Me_3TTF-PO_3H_2$. An ESR signal with a g value centered around 2.007 is observed from a powder sample, and the spin susceptibility (Fig. 1) obtained by variable

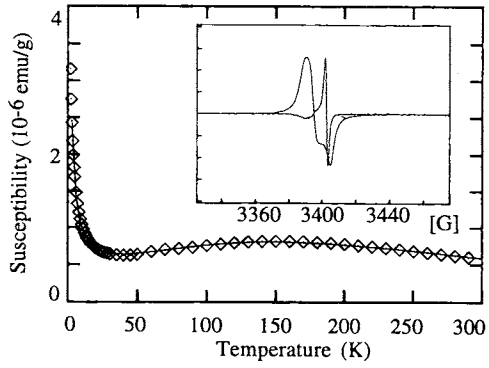

Fig. 1. Magnetic susceptibility of $[Me_3TTF\ PO_3H_2$ (**4**), $Me_3TTF-PO_3H^-]^+$ (**5**) as a function of temperature, measured with a SQUID magnetometer operating at 1 T. The solid line represents the fit of the data to $\chi = \chi_{BF} + C/T + \chi_{dia}$ (see text). Insert: ESR spectrum of a powdered sample of **5** at 290 K with diphenylpicrylhydrazine (DPPH) as a reference.

temperature DC magnetization measurements is characteristic of uniform, antiferromagnetically coupled discrete chains of spins and fits the appropriate Bonner–Fisher expression for spins $S = {}^1/_2$ well.[13] The fit to the data represented by the solid line in Figure 1 provides the large intrachain coupling integral value J/k of 120 K, which indicates strong antiferromagnetic interactions. Furthermore, the presence of one spin for two molecules is deduced. Therefore we conclude that the hydrolysis of **3** yields the mixed valence compound, **5**, formulated as $[Me_3TTF-PO_3H_2, Me_3TTF-PO_3H^-]^+$,[14] whose formation deserves special comment.

First, note that the observed high sensitivity of the trimethyltetrathiafulvalenylphosphonic acid (**4**) to air oxidation is quite surprising, since one expects the electrochemical behavior of the free diacid **4** to be similar to that of the diester **2**, which turns out to be oxidized at potentials even higher ($E^1_{1/2}$ = 0.495 V vs. ECS) than Me_3TTF itself (0.36 V vs. ECS). In that respect, the propensity of TTF solutions to generate paramagnetic species in the presence of strong acids has been recently emphasized by Gorgues et al., who also demonstrated that the central double bond of the TTF core is readily protonated under those conditions.[15a] In addition, note that the trimethyltetrathiafulvalenylphosphonic acid **4** is indeed expected to be as strong an acid as any aromatic phosphonic acid; for example, the pKa_1 for phenylphosphonic acid is 1.85.[16] Therefore, we conclude that the air oxidation of **4** is catalyzed by its self-supported strong acid functionality following a mechanism related to Gorgues' protonation mechanism.[15b] Thus, the concomitant neutralization of the first phosphonic acid proton and reduction of **5** with aniline yields the stable parent anilinium salt **6**.

X-ray crystal structure of 6, an organic lamellar phosphonate with an anti-$CaSi_2$ framework: The atom numbering scheme is shown in Figure 2 together with the structures of the molecular ions. It

Abstract in French: *L'acide triméthyltétrathiafulvalénylphosphonique $Me_3TTF-PO_3H_2$ (TTF: tétrathiafulvalène) est obtenu sous forme partiellement oxydée par réaction de $Me_3TTF-Li$ avec $ClPO(OEt)_2$ suivie d'une hydrolyse par Me_3SiBr. Le sel de monoanilinium du phosphonate correspondant est obtenu par réduction et neutralisation par l'aniline. Un réseau hexagonal de liaisons hydrogène est identifié au sein de la structure lamellaire de $[PhNH_3^+][Me_3TTF-PO(OH)O^-]$ dont l'analogie au type structural anti-$CaSi_2$ est soulignée. Des monocristaux du radical neutre zwitterrionique $[Me_3TTF-PO(OH)O^-]^{\cdot+}$ sont obtenus par électrocristallisation de solutions du phosphonate d'anilinium. L'analyse de leur structure permet de mettre en évidence des rubans moléculaires créés par l'association des radicaux neutres par liaisons hydrogène. L'empilement de ces rubans génère une nouvelle architecture bidimensionnelle qui rappelle celles rencontrées dans des sels de cations radicaux de donneurs π de plus grande extension spatiale. L'analyse des énergies de recouvrement entre les HOMO des radicaux neutres démontre l'existence de fortes interactions intermoléculaires de type π–π au sein des feuillets en dépit de l'absence de réseau bidimensionnel de contacts courts S···S. La susceptibilité de spin de $[Me_3TTF-PO(OH)O^-]^{\cdot+}$, déterminée par résonance électronique sur monocristal, démontre la présence d'excitons triplet dont l'origine est interprétée en fonction de la structure électronique du composé.*

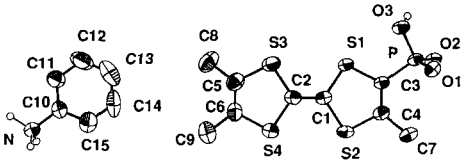

Fig. 2. ORTEP diagram showing the individual components in $[PhNH_3^+][Me_3TTF\text{-}PO(OH)O^-]$ (**6**) with 50% probability thermal ellipsoids. Hydrogen atoms on the methyl groups have been omitted for clarity. Selected bond lengths (Å) and angles (°): S1–C1 1.754(5), S1–C3 1.755(5), S2–C1 1.753(5), S2–C4 1.753(5), S3–C2 1.753(5), S3–C5 1.741(6), S4–C2 1.752(6), S4–C6 1.751(6), C1–C2 1.329(8), C3–C4 1.325(7), C5–C6 1.328(9), C3–P 1.798(5), P–O1 1.491(4), P–O2 1.508(3), P–O3 1.564(3), O3–H3 0.930(3); S1-C3-P 116.4(3), C4-C3-P 126.2(4), C3-P-O1 108.4(2), C3-P-O2 109.0(2), C3-P-O3 102.7(2), O1-P-O2 115.7(2), O1-P-O3 108.9(2), O2-P-O3 111.3(2), P-O3-H3 103.0(2).

should be noted that the hydrogen atoms have been unambigously located on the Fourier difference maps. The presence of one hydrogen atom on O3 and the fact that the P–O1 and P–O2 bond lengths are shorter than that of P–O3 (1.491, 1.508, and 1.564 Å, respectively) confirm that the phosphonic acid is monodeprotonated. The TTF core is quasiplanar and the coordination geometry around the phosphorus atom is essentially tetrahedral. As exemplified in Figure 3, the construction

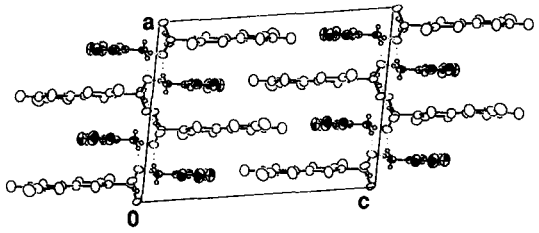

Fig. 3. A projection of the structure of $[PhNH_3^+][Me_3TTF\text{-}PO(OH)O^-]$ (**6**) along *b* showing the interdigitated planar organic molecules and providing a first glance at the hydrogen-bond network on the outskirts of the inner hydrophobic organic slab.

of the unique layered structure of $[PhNH_3^+][Me_3TTF\text{-}PO(OH)O^-]$ (**6**) results from the interplay between i) the association of the hydrophilic groups PO_3H^- and NH_3^+ within a remarkable two-dimensional pattern in the (*a*,*b*) plane, and ii) the neat complementary interdigitated arrangement of the quasiparallel hydrophobic phenyl and trimethyltetrathiafulvalenyl planes (separated by 3.64(1) Å). While the latter is already plainly apparent in Figure 3, the former is best described by considering the partial projection of structure onto the (*a*,*b*) plane, shown in Figure 4a. The phosphonate oxygen atom O3 is hydrogen-bonded with the phosphonate oxygen atom O2′ of a neighboring molecule. This creates a centrosymmetrical dimeric unit, a $R_2^2(8)$ ring in Etter's notation,[4] typical of carboxylic acid structures. Each centrosymmetrical phosphonate dimer is surrounded by and hydrogen-bonded to six anilinium molecules with the strong hydrogen bonds shown by dotted lines in Figure 4a and described in Table 1. A striking hexagonal

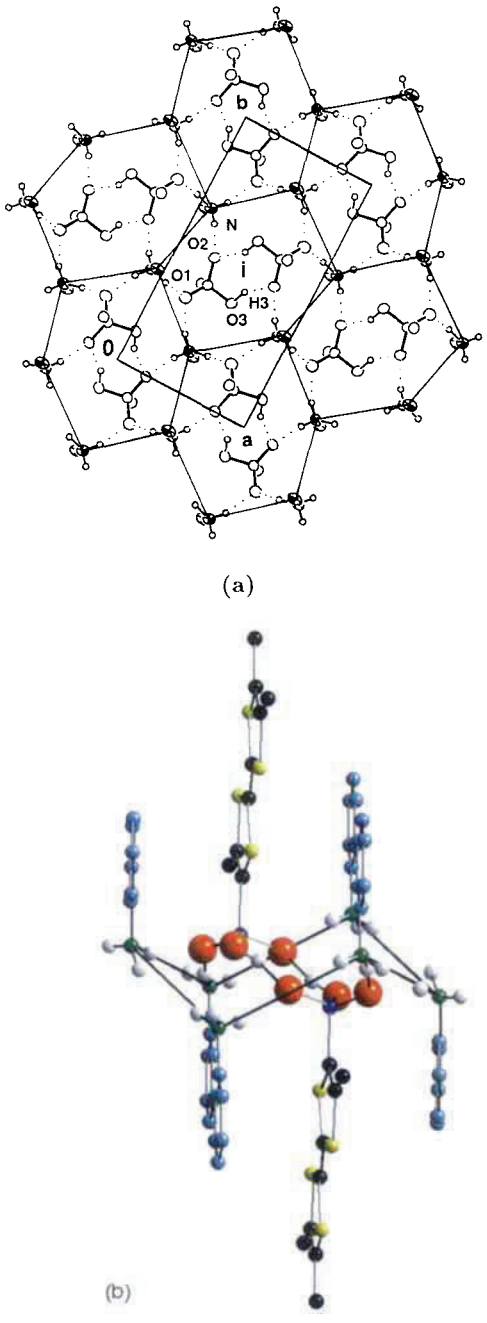

Fig. 4. a) A projection of only the $C10NH_3^+$ and $C3PO_3H^-$ groups of one single hydrophilic layer onto the (*a*,*b*) plane in the crystal structure of **6**. The set of hydrogen bonds collected in Table 1 is shown by dotted lines. Note the hexagonal honeycomb pattern drawn by the solid lines connecting the nitrogen atoms. The cyclohexane-like motif is slightly irregular to allow for the proper nesting of the $R_3^3(8)$ ring within its inner cavity: thus, the opposite edges of the motif parallel to the plane of Figure 4b are slightly longer (5.213 Å) than the other four (4.954 Å). b) A perspective view of one cyclohexane-like motif (for example, the inner motif in Fig. 4a) connecting the nitrogen atoms looking along a direction close to the plane of Figure 4a; the structure illustrates i) the chair-like conformation of the motif and ii) the inner $R_3^3(8)$ ring. N: green; H: white; anilinium C's: light blue; O: red; P: dark blue; S: yellow; trimethyltetrathiafulvalene C's: black.

Table 1. Selected hydrogen bond lengths (Å) and angles (°) in **6**.

	H···O	O(N)···O	O(N)–H···O
N–H1a···O2	1.990(1)	2.800(2)	158.43(1)
N–H1b···O1	1.870(1)	2.762(2)	154.89(1)
N–H1c···O1	1.601(1)	2.743(2)	170.87(1)
O3–H3···O2	1.689(1)	2.545(2)	151.73(1)

net is revealed by connecting the nitrogen atoms of the ammonium cations within the projection in Figure 4a. The geometry of the generic motif shown in Figure 4b in a perspective view is reminiscent of that of cyclohexane in its chair conformation. Furthermore, as shown in Figure 5, the extended, puckered two-dimensional net, initially viewed in projection (Fig. 4a), is similar to the layer pattern of the α-As structure, that is, the simplest

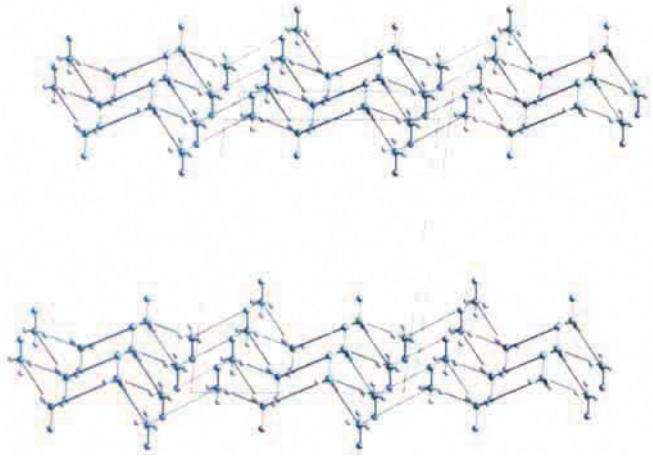

Fig. 5. The extended puckered hexagonal net developing within the hydrophilic interface in the lamellar architecture of **6**, exemplifying the analogy with the α-As structure or the Si hexagonal nets within the prototypical layered structure $CaSi_2$. The *a* axis runs horizontally and the *c* axis vertically.

3-connected plane net one can possibly construct (here, the structure generator is NH_3^+). To take this structural analogy further, the proper structural prototype for **6** is the $CaSi_2$ structure[17] depicted in Figure 6. Indeed, the structure of **6** is best

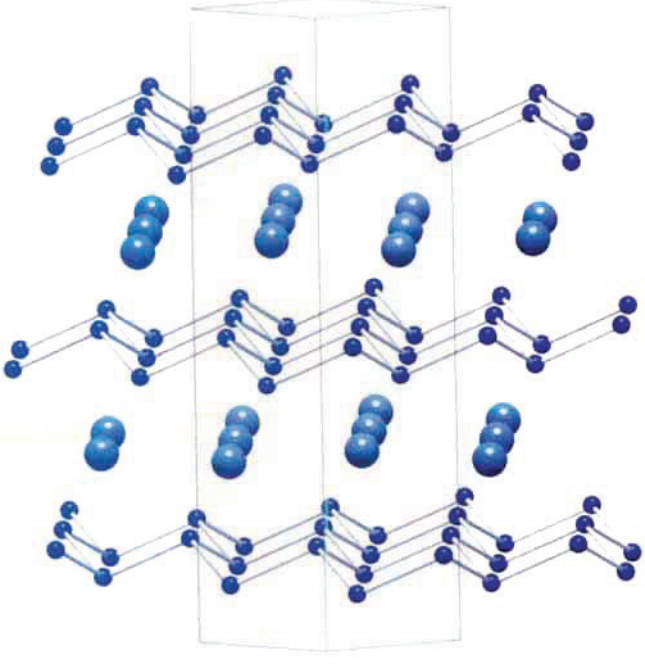

Fig. 6. A view of the $CaSi_2$ structure. Ca: large light blue circles; Si: small dark blue circles.

thought of as belonging to the anti-$CaSi_2$ structure type, where the anilinium cations form three hydrogen bonds and act as Si^-, and two trimethyltetrathiafulvalenephosphonate anions connect the layers (Fig. 7) by analogy with the role of Ca^{2+} (Fig. 6). This structural analysis provides a rationale for the unique lamellar character of the structure of **6**, further depicted in Figure 8. It should be noted that, while numerous organic phosphonate salts such as α-ZrP,[3] for example, present a typical layered structure as the result of coordination of the phosphonate moieties on the metal cations,[7] the lamellar character of **6** has been achieved in a purely organic system by making use of directional

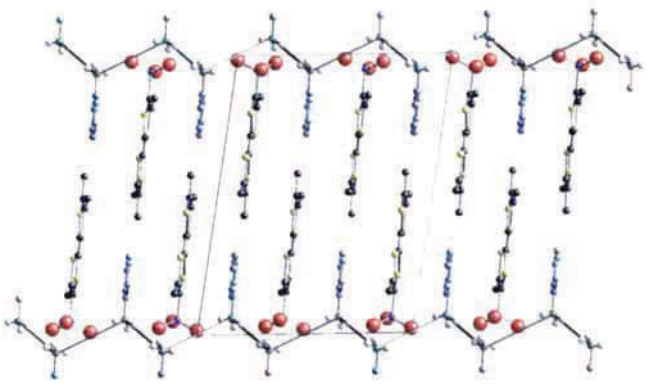

Fig. 7. Relative anchoring of the extended hexagonal nets in **6** by the neat assembly of the hydrophobic organic fragments. Compare with the registry of the (Si^-), slabs by the Ca^{2+} ions in trigonal prismatic sites in Figure 6. The *a* axis runs horizontally and the *c* axis vertically.

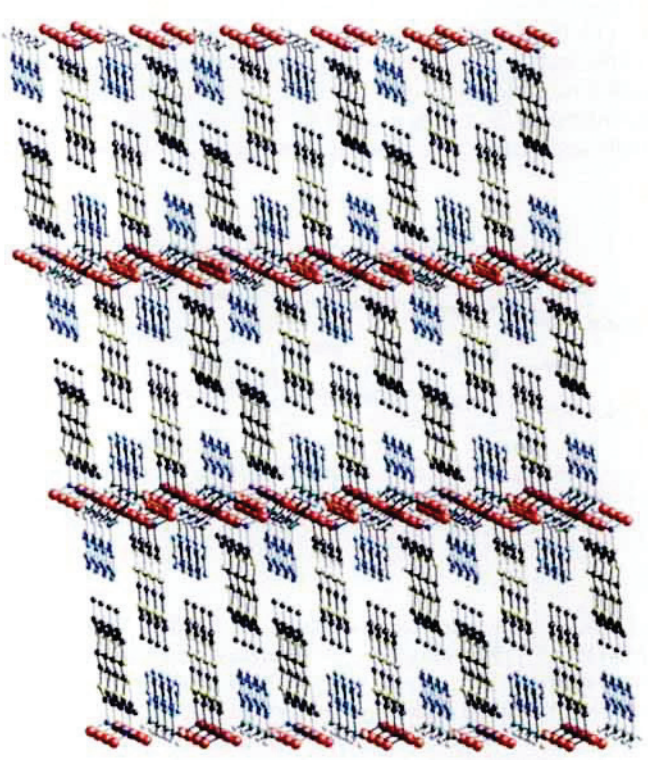

Fig. 8. A fully reconstructed view of the crystal structure of **6** illustrating its remarkable lamellar character.

intermolecular interactions such as hydrogen bonds as well as shape complementarity principles to control solid state organization, an issue of considerable present interest.[5, 18] The lamellar organization of **6** (Fig. 8) is also reminiscent of the alkylammonium dihydrogen phosphate bilayer pattern observed in vesicle templates involved in mesoscale pattern formation.[19]

The neutral π radical $[Me_3TTF-PO(OH)O^-]^{\cdot+}$ (7): The cyclic voltammogram of **6** in dimethylformamide exhibits two reversible oxidation waves at 0.35 and 0.61 V vs. SCE. This qualifies the trimethyltetrathiafulvalenephosphonate anion as an excellent π-donor molecule comparable to Me_3TTF itself (0.365 and 0.635 V vs. SCE in DMF), and also demonstrates that the anionic character of the molecule essentially compensates for the electron-withdrawing effect of the phosphonic acid group since $Me_3TTF-PO(OEt)_2$ is reversibly oxidized at 0.495 and 0.725 V vs. SCE, also in DMF.

0947-6539/96/0210-1278 $ 15.00+.25/0 Chem. Eur. J. 1996, 2, No. 10

The opportunity to isolate a zwitterionic radical by oxidation of the TTF core in **6** is thus offered. Indeed, the electrocrystallization of DMF solutions of **6** (Scheme 1) provided good-quality single crystals of $[Me_3TTF-PO(OH)O^-]^{\cdot+}$ (**7**), as expected.

X-ray crystal structure of 7: An ORTEP diagram of $[Me_3TTF-PO(OH)O^-]^{\cdot+}$ is shown in Figure 9. Note the quasiplanarity of the molecule. From a structural point of view, two major features will serve to identify the charge in this TTF phosphonic acid. First, a comparison of the C=C and C–S intramolecular bond lengths in **7**, which are particularly sensitive to the charge on the TTF core,[20] with those for $Me_3TTF-PO(OH)O^-$ in **6** (Fig. 2) suggests that the TTF core is fully oxidized in **7**. Secondly, the average P–O bond length (1.516 Å) in **7**, which is correlated with the charge on the PO_3H_2 substituent,[21] is very similar to that observed in **6** (1.522 Å), thus leading to the conclusion that this substituent is also monodeprotonated. Therefore, both charges (positive on the TTF core, negative on the substituent; see Scheme 1) compensate within the same molecule, also of course in agreement with the identification of one single molecular component within the crystal lattice. To our knowledge, this molecule is the first example of a properly characterized zwitterionic TTF-based π radical. It is true that the existence of the internal salt $[TTF-COO^-]^+$ has already been reported[22] but, as shown elsewhere,[23] this salt is unstable and is readily decarboxylated. Since the P–O1 and P–O3 bonds are longer than the P–O2 bond (1.522(6), 1.523(5), and 1.503(7) Å, respectively), it is likely that the single hydrogen atom on the phosphonate group (which could not be identified on the Fourier difference map) is disordered on both oxygen atoms O1 and O3 in the solid state. The use of the methodology of structure levels developed to simplify and categorize the complex structural hierarchy of proteins permits a convenient description of the crystal structure of **7**.[24] Thus, the primary structure (shown in Fig. 10a) consists of two hydrogen-bond patterns, the dimer D and the ring $R_2^2(8)$ of Etter's classification,[4] between neighboring phosphonate molecules. Note that the O···O distances within both D and $R_2^2(8)$ are particularly short (O1···O1 = 2.411(5) and O2···O3 = 2.491(5) Å), indicating strong hydrogen bonding.[25] Note also that the single available proton is disordered and distributed within these series of hydrogen bonds in the solid. The secondary structure is identified as the association of the alternating dimers D and rings $R_2^2(8)$ along *a* that form the backbone of one-dimensional hydrogen-bonded ribbons, depicted in Figure 10b. The supersecondary structure is then defined as the packing of these ribbons; this again creates a novel layered architecture, as shown in Figure 11. Note that the latter pattern is unprecedented for a molecule essentially similar to tetramethyltetrathiafulvalene (TMTTF), whose radical cation salts only form one-dimensional structures. Indeed, such two-dimensional layered arrangements are typically achieved in radical cation salts of π-donor molecules of larger spatial extension such as the prototypical bis(ethylenedithio)-tetrathiafulvalene (BEDT–TTF), as discussed below.

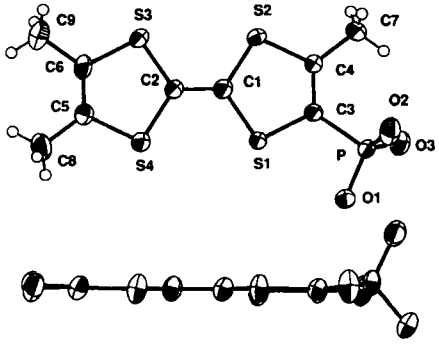

Fig. 9. ORTEP view (50% probability thermal ellipsoids) of the neutral π radical in the crystal structure of $[Me_3TTF-PO(OH)O^-]^{\cdot+}$ (**7**). Selected bond lengths (Å) and angles (°): S1–C1 1.743(7), S1–C3 1.732(7), S2–C1 1.731(8), S2–C4 1.748(7), S3–C2 1.724(7), S3–C6 1.756(8), S4–C2 1.741(8), S4–C5 1.747(7), C1–C2 1.36(1), C3–C4 1.364(9), C5–C6 1.33(1), C3–P 1.800(6), P–O1 1.522(6), P–O2 1.503(7), P–O3 1.523(5); S1-C3-P 117.0(4), C4-C3-P 125.4(6), C3-P-O1 102.3(3), C3-P-O2 107.8(3), C3-P-O3 107.9(3), O1-P-O2 113.5(3), O1-P-O3 112.5(3), O2-P-O3 112.1(3).

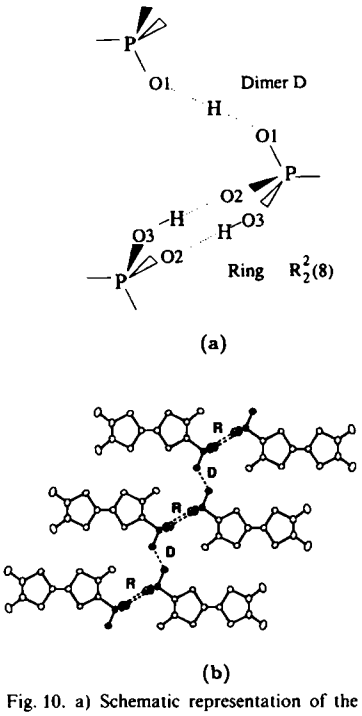

Fig. 10. a) Schematic representation of the hydrogen bond motifs in **7** (primary structure). b) The ribbon motif of the secondary structure.

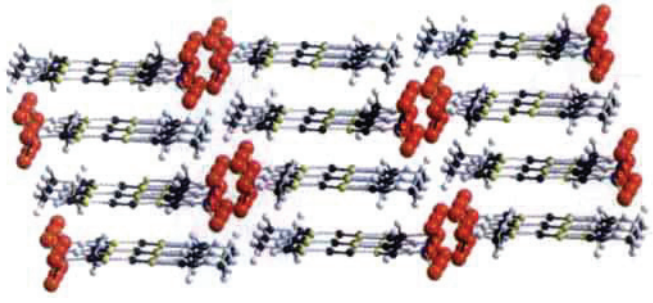

Fig. 11. Identification of slabs of neutral π-radical molecules in the crystal structure of **7**, a consequence of the interdigitated layering of the ribbons (supersecondary structure).

A unique two-dimensional electronic structure with no conventional S···S π-orbital overlap: No conventional π–π interactions resulting from short S···S distances can be detected between each superposed ribbon. The shortest intermolecular S···S distances are 3.712, 3.791, and 3.987 Å, which are longer than the sum of the van der Waals radii. Despite this lack of S···S contacts, the calculated HOMO–HOMO[26] intermolecular interaction energies,[27] which are a measure of the strength of the interaction between two HOMOs in adjacent positions of the lattice, are large. This suggests that there are indeed important π–π interactions between the ribbons. The five HOMO–HOMO intermolecular interaction energies (I to V, see Fig. 12a) calculated for **7** are given in Table 2. These values are comparable in magnitude to those found in many metallic charge-transfer salts of BEDT–TTF (ET for short), for instance, the values of the five different HOMO–HOMO intermolecular interaction energies for the donor slabs of metallic β-$(ET)_2I_3$ that we report in Table 2 (see the schematic view of such donor slabs,

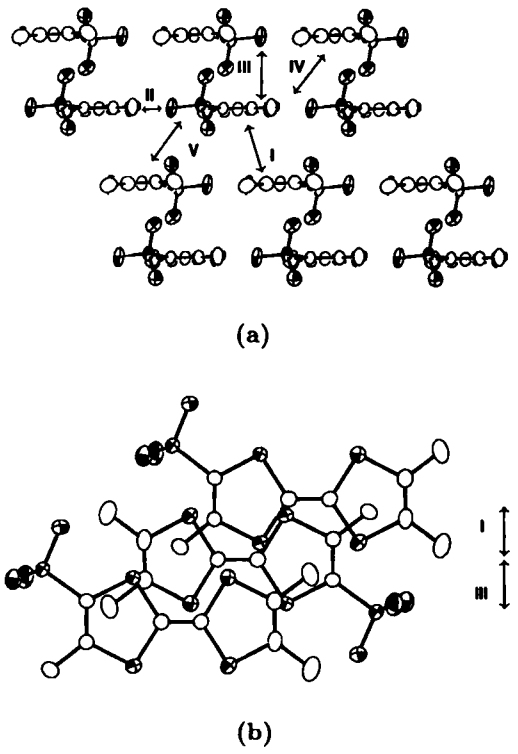

Fig. 12. a) A projection of one single slab in 7 along the long molecular axis of the TTF core. b) Intermolecular overlap along the stack in one slab, showing the very strong σ-type interactions between some S and C π orbitals.

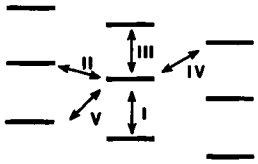

Scheme 2, which is rather like the projection shown in Fig. 12a, where every line represents an ET donor viewed along the long axis of the molecule).[28] The similarity between the two series of intermolecular interaction energies is clear. In fact, those for 7 are even somewhat larger. Thus, from an electronic viewpoint we find a slab in 7 which is not so unlike those found in the well-known β-$(ET)_2X$ family.[27b] Although geometrically the two slabs are somewhat different, in both cases there are chains of molecules with strong interactions of alternating strength ($\cdots$I$\cdots$III$\cdots$I$\cdots$III$\cdots$), and these chains are coupled through interactions of smaller but far from negligible strength along another direction ($\cdots$IV$\cdots$V$\cdots$IV$\cdots$V$\cdots$). As a matter of fact, the interchain coupling is even stronger in the present case.

It is clear that 7 contains slabs with strong $\pi-\pi$ intermolecular interactions despite the nonexistence of a 2D network of short S$\cdots$S contacts. It should be noted that the four substituents make practically no contribution to the HOMO of 7 and, consequently, the calculated HOMO–HOMO interaction energies of Table 2 result only from the inner core of the molecule. Although traditionally only S$\cdots$S contacts have been considered when looking at the existence of intermolecular interactions in charge-transfer salts, it should be recalled that the HOMO is a delocalized orbital and contains important contributions from other atoms (the central C atoms in the present case). For instance, the particularly strong HOMO–HOMO interactions along the stacks defined by I and III (Fig. 12a) are the result of very strong σ-type interactions between S and C π orbitals which are nearly on top of each other, as shown in Figure 12b. Thus, S$\cdots$C interactions can also be very important if their associated π orbitals are properly oriented. We wish to stress the importance of discussing the strength of intermolecular interactions on the basis of HOMO–HOMO intermolecular interaction energies and not solely on the basis of short S$\cdots$S contacts.

Table 2. HOMO–HOMO Interaction energies (eV) calculated for 7 and β-$(ET)_2I_3$.

Interaction	7 [a]	β-$(ET)_2I_3$ [b]
I	0.317	0.287
II	0.075	0.024
III	0.394	0.439
IV	0.177	0.066
V	0.192	0.164

[a] See Figure 12a for labeling. [b] See Scheme 2 for labeling.

Each of the two HOMO bands of 7 are approximately 0.6 eV wide; in agreement with our previous discussion, this is almost the same dispersion calculated for the HOMO bands of β-$(ET)_2I_3$.[29] The two bands overlap slightly so that the system could be formally considered as a semimetal. However, since the compound is insulating, we are led to the conclusion that the electrons in 7 are localized, with one electron on each zwitterionic radical. The situation is formally the same as for 1:1 charge-transfer salts in which, despite the existence of a half-filled band according to the one-electron approach, the electrons are localized with one electron in each site of the lattice. Opportunities are now offered to react the material with electron donors in order to stabilize the metallic state by doping the energy band away from formal half-filling, an approach resembling that employed by Haddon to generate iodine-doped salts of the neutral benzene-bridged bis(dithiadiazolyl) diradicals.[30]

Magnetic properties of 7: A single anisotropic Lorentzian line with a g value of 2.0082, typical of TTF-based radical cations, is observed by room-temperature ESR on a single crystal oriented with its long axis parallel to the field. The $\ln(\chi T)$ vs. T^{-1} curve (where χ is the spin susceptibility normalized to the room-temperature value) and the temperature dependence of the ESR linewidth are given in Figure 13. A high-temperature regime is identified in which the spin susceptibility follows an exponential law characteristic of a thermally activated process [Equation (1), with

$$\chi = \chi_0 \exp(-J_1/kT) \quad (1)$$

$J_1/k = 436$ K]. Below 100 K, the slope of the curve in Figure 13a decreases to the value $J_2/k = 121$ K. This abrupt change of slope corresponds to the appearence of a narrower resonance line superposed on the resonance line that was present at high temperature and had progressively disappeared (Fig. 13b). This behavior is typical of triplet excitons.[20a, 31] In the high-temperature regime ($T > 100$ K), the single resonance line is the triplet exciton line, which is averaged because of the collisions be-

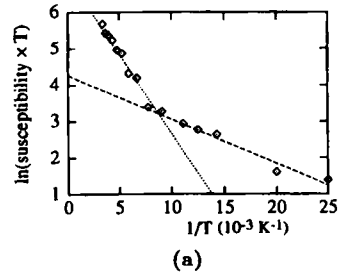

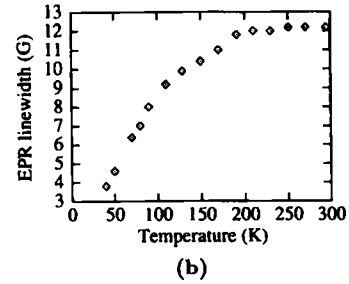

Fig. 13. a) $\ln(\chi T)$ as a function of the inverse temperature and b) the ESR linewidth as a function of temperature for a single crystal of 7 in an arbitrary orientation position within the resonance cavity.

0947-6539/96/0210-1280 $ 15.00+.25/0 Chem. Eur. J. 1996, 2, No. 10

tween the excitons,[32] and at low temperature only the impurity line, a common feature of such systems,[33] remains present. Note that the somewhat low value of J/k is in agreement with the fact that the triplet state is highly populated, thus leading to collisions between the numerous excitons. This particular magnetic response of the material was nevertheless somewhat unexpected, since it suggests the presence of weakly interacting dimers within the slabs in **7** where the presence of localized, perhaps essentially noninteracting spins localized on each zwitterion site was expected to yield either a Curie-type spin susceptibility or perhaps indications for low-dimensional antiferromagnetic fluctuations. The former analysis of the electronic structure of the slab in **7** provides an explanation of the observed spin susceptibility. It is very likely that the singlet–triplet excitons originate in the dimers formed by the zwitterion molecules interacting along the stack, particularly across the type III interaction (Fig. 13), the strongest among the five HOMO–HOMO interaction energies (Table 2).

Experimental Section

$Me_3TTF-P(O)(OEt)_2$ (2): To a solution of **1** (1 g, 4.06 mmol) in dry Et_2O (100 mL) kept at −78 °C under nitrogen was added in turn $NH(iPr)_2$ (0.64 mL, 4.46 mmol) and BuLi (2.5 M in hexanes, 1.8 mL, 4.46 mmol). The suspension was stirred for 1 h and $(EtO)_2P(O)Cl$ (0.65 mL, 4.46 mmol) was added. The yellow mixture turned orange immediately. The solution was slowly warmed up to room temperature. The solvent was evaporated, 100 mL of dichloromethane and 100 mL of water were added to the residue, and the organic layer was dried over $MgSO_4$ and concentrated. Chromatography (silica gel, dichloromethane) afforded first the unreacted trimethyltetrathiafulvalene, followed by the diester **2**. The resulting oil crystallized in the flask and the orange solid was then triturated in pentane and filtered off to yield 0.85 g of **2**; yield 50%. M.p. 120–121 °C; ^1H NMR (200 MHz, [D$_6$]DMSO): $\delta = 1.26$ (t, $^3J(H,H) = 7.03$ Hz, 6H, CH_2CH_3), 1.95 (s, 6H, $ArCH_3$), 2.28 (d, $^4J(H,P) = 2.67$ Hz, 3H, $ArCH_3$), 4.05 (sextet, $^3J(H,P) = 8.50$ Hz, $^3J(H,H) = 7.03$ Hz, 4H, CH_2CH_3); $^{31}P\{^1H\}$ NMR (200 MHz, CH_2Cl_2, H_3PO_4 85%): $\delta = 7.09$; anal. calcd for $C_{13}H_{19}O_3PS_4$: C 40.84, H 4.37, P 8.11, S 33.51; found: C 40.74, H 5.11, P 7.95, S 33.34.

$[Me_3TTF-P(O)(OH)_2]_{ox}$ (5): To a solution of **2** (0.85 g, 2.22 mmol) in 20 mL of dry dichloromethane under nitrogen was added Me_3SiBr (2.4 mL, 8.88 mmol) and NEt_3 (0.8 mL, 8.88 mmol). The solution was stirred for 6 h and the solvent evaporated in vacuo. To the resulting solid **3** was added methanol (20 mL). The solution was stirred for another 6 h until the starting material has totally disappeared (TLC). A dark brown precipitate was filtered, washed with water and ethanol, and dried; anal. calcd for $C_9H_{11}O_3PS_4$: C 33.12, H 3.39, P 9.49, S 39.29, Si 0; found: C 33.16, H 3.36, P 8.89, S 38.35, Si 0.20. The small amounts of Si detected may indicate the presence of the partially hydrolyzed compound $Me_3TTF-P(O)(OSiMe_3)(OH)$.

$[PhNH_3^+][Me_3TTF-PO(OH)O^-]$ (6): Aniline (10 mL, 10.8 mmol) was added to a suspension of **5** (0.30 g, 0.92 mmol) in methanol (50 mL). The solution was stirred over a steam bath at 50 °C for 1 h. The dark solid slowly dissolved and the solution turned orange. The methanol was then evaporated and the salt was precipitated by addition of Et_2O. Recrystallization from MeOH/acetone (4:1) afforded 0.22 g of **5** as orange crystals; yield 57%. M.p. 276–278 °C (decomp.); ^1H NMR (200 MHz, [D$_6$]DMSO): $\delta = 1.93$ (s, 6H, CH_3), 2.21 (s, 3H, CH_3), 6.78 (m, 5H, ArH); $^{31}P\{^1H\}$ NMR (200 MHz, CH_2Cl_2, H_3PO_4 85%): $\delta = 2.38$; anal. calcd for $C_{15}H_{18}NO_3PS_4$: C 42.94, H 4.32, N 3.34, P 7.38, S 30.57; found: C 42.16, H 4.31, N 3.28, P 6.51, S 30.52.

$[Me_3TTF-PO(OH)O^-]^+$ (7): Black, shiny platelets of **7** were grown at 25 °C for 7 days at a platinum wire anode under constant-current electrolysis ($I = 0.2$ μA) of a DMF solution (10 mL) of **6** (8 mg) containing 200 mg of tetrabutylammonium perchlorate as electrolyte. The solvent was stirred overnight over basic aluminum oxide and distilled under vacuum before use.

Electrochemical measurements: Cyclic voltammograms were recorded with a PAR 273 potentiostat with Pt working (1 mm^2) and auxiliary (1 cm^2) electrodes, a SCE reference electrode, and $(nBu)_4N^+PF_6^-$ as the supporting electrolyte. Solvents were dried over basic aluminum oxide before use.

X-ray structure determination of compounds 6 and 7: Reflections were measured on an Enraf–Nonius CAD4 diffractometer, with graphite-monochromated $Mo_{K\alpha}$ radiation ($\lambda = 0.7107$ Å, $\omega/2\theta$ scan mode). Measured intensities were corrected for Lorentz and polarization effects. Absorption corrections were applied for **7** by means of empirical procedures based on azimuthal ψ scans of some reflections having an Eulerian angle χ near 90°. The structures were solved by direct methods and refined with full-matrix least-squares methods with unit weights for **6** and the weighting scheme $1/w = [\sigma^2(I) + (0.07F_o^2)^2]/4F_o^2$ with $\sigma(I)$ from counting statistics for **7**. All the calculations were performed on an IBM RS/6000 computer with the Xtal 3.2 system of programs [34]. The crystallographic data for **6** and **7** is summarized in Table 3 [35].

Table 3. Crystal data for **6** and **7**.

	6	**7**
chemical formula	$C_{15}H_{18}NO_3PS_4$	$C_9H_{10}O_3PS_4$
formula weight	419.53	325.39
T (K)	293	293
space group	$P2_1/a$	$P\bar{1}$
a (Å)	14.135(1)	7.610(4)
b (Å)	7.462(1)	12.030(3)
c (Å)	18.468(1)	7.480(2)
α (°)	90	101.77(2)
β (°)	99.37(1)	104.57(3)
γ (°)	90	79.89(3)
V (Å^3)	1921.9(3)	643(1)
Z	4	2
ρ_{calcd} (g cm^{-3})	1.45	1.68
μ (cm^{-1})	5.9	8.5
crystal size	0.06 × 0.33 × 0.50	0.04 × 0.17 × 0.23
octants collected	$\pm h, k, l$	$h, \pm k, \pm l$
max. h, k, l	17, 9, 22	9, 14, 9
2θ range	2, 26	2, 26
no. of reflns collected	4028	2823
no of unique reflns	3763	2520
no. of reflns used ($I > 3\sigma(I)$)	1991	1373
no. of variables	217	154
R [a], Rw [b]	0.046, 0.044	0.070, 0.092
max peak on final diff Four. map (e Å^{-3})	0.59	1.08
GoF [c]	1.43	1.15

[a] $R = \sum||F_o| - |F_c||/\sum|F_o|$. [b] $R_w = [\sum w(|F_o| - |F_c|)^2/\sum|F_o|^2]^{1/2}$. [c] $S = [\sum w(F_o^2 - F_c^2)^2/(N_{observations} - N_{variables})]^{1/2}$.

ESR measurements: Single-crystal temperature-dependent ESR measurements were performed on a Varian X-band spectrometer operating at 9.3 GHz and equipped with an Oxford ESR 900 helium cryostat. The spin susceptibility is determined by numerical double integration with an attenuation of 15 dB to avoid saturation.

Magnetic susceptibility studies: Magnetic susceptibility measurements on powder samples of **5** were made with a Quantum Design MPMS-5 SQUID magnetometer operating at 1 T in the range 1.7–400 K.

Band structure calculations: The tight-binding band structure calculations are based upon the effective one-electron Hamiltonian of the extended Hückel method [36]. The off-diagonal matrix elements of the Hamiltonian were calculated according to the modified Wolfsberg–Helmholz formula [37]. The basis set consisted of double-ζ Slater-type orbitals for C, P, O, and S and single-ζ Slater-type orbitals for H. The exponents (ζ_μ, ζ'_μ), contraction coefficients (c_μ, c'_μ) and atomic parameters ($H_{\mu\mu}$) used for C, S, and H were taken from previous work [1]. The values employed for P and O were 2.367, 1.499, 0.5846, 0.5287, and −19.0 eV for P 3s; 2.064, 1.227, 0.4908, 0.5940, and −12.0 eV for P 3p; 2.688, 1.675, 0.7076, 0.3745, and −32.3 eV for O 2s and 3.694, 1.659, 0.3322, 0.7448, and −14.8 eV for O 2p.

Acknowledgments: We thank the CNRS and the Région des Pays de Loire for support. E. C. would like to thank the CNRS for a sabbatical leave that made the stay at ICMAB possible.

Received: February 28, 1996 [F310]

[1] The layered compounds might have direct electronic functions such as metallic conductivity or superconductivity. See A. Pénicaud, K. Boubekeur, P. Batail, E. Canadell, P. Auban-Senzier, D. Jérôme, *J. Am. Chem. Soc.* **1993**, *115*, 4101, and leading references therein to the field of two-dimensional molecular conductors and superconductors.

[2] The use of layered molecular compounds in electrooptics indirectly depends on their dielectric properties. See H. E. Katz, M. L. Schilling, *Chem. Mater.* **1993**, *5*, 1162.

[3] This is particularly true in the field of layered and pillared zirconium phosphonates: see *Soft Chemistry Routes to New Materials* (Eds.: J. Rouxel, M. Tournoux, R. Brec), Trans Tech, Aedermanndorf (Switzerland), **1994**.

[4] a) M. C. Etter, *Acc. Chem. Res.* **1990**, *23*, 120; b) J. Bernstein, M. C. Etter, L. Leiserowitz in *Structure Correlation, Vol. 2* (Eds.: H.-B. Bürgi, J. D. Dunitz), VCH, Weinheim, **1994**, pp. 431–507.
[5] a) Y.-L. Chang, M.-A. West, F. W. Fowler, J. W. Lauher, *J. Am. Chem. Soc.* **1993**, *115*, 5991; b) J. C. MacDonald, G. M. Whitesides, *Chem. Rev.* **1994**, *94*, 2383.
[6] See, for example, P. N. W. Baxter, J.-M. Lehn, J. Fischer, M.-T. Youinou, *Angew. Chem.* **1994**, *106*, 2432; *Angew. Chem. Int. Ed. Engl.* **1994**, *33*, 2284.
[7] See, for example, a) G. Huan, A. J. Jacobson, J. W. Johnson, E. W. Corcoran, *Chem. Mater.* **1990**, *2*, 91; b) G. Cao, V. M. Lynch, J. S. Swinnea, T. E. Mallouk, *Inorg. Chem.* **1990**, *29*, 2112; c) J. Le Bideau, B. Bujoli, A. Jouanneaux, C. Payen, P. Palvadeau, J. Rouxel, *ibid.* **1993**, *22*, 4617; d) G. Alberti, F. Marmottini, S. Murcia-Mascaros, R. Vivani, *Angew. Chem.* **1994**, *106*, 1655; *Angew. Chem. Int. Ed. Engl.* **1994**, *33*, 1594; e) M. I. Khan, Y.-S. Lee, C. J. O'Connor, R. C. Haushalter, J. Zubieta, *J. Am. Chem. Soc.* **1994**, *116*, 4525; f) H. Byrd, S. Whipps, J. K. Pike, J. Ma, S. E. Nagler, D. R. Talham, *ibid.* **1994**, *116*, 295; g) H. E. Katz, W. L. Wilson, G. Scheller, *ibid.* **1994**, *116*, 6636; h) H. E. Katz, *Chem. Mater.* **1994**, *6*, 2227; i) M. I. Khan, J. Zubieta in *Early Transition Metal Clusters with π-Donor Ligands* (Ed.: M. H. Chisholm), VCH, Weinheim, **1995**, pp. 247–283.
[8] See a) P. Blanchard, K. Boubekeur, M. Sallé, G. Duguay, M. Jubault, A. Gorgues, J. D. Martin, E. Canadell, P. Auban-Senzier, D. Jérôme, P. Batail, *Adv. Mater.* **1992**, *4*, 579; b) M. Sallé, M. Jubault, A. Gorgues, K. Boubekeur, M. Fourmigué, P. Batail, E. Canadell, *Chem. Mater.* **1993**, *5*, 1196; c) M. R. Bryce, *J. Mater. Chem.* **1995**, *5*, 1481; d) H. Mayaffre, P. Wzietek, C. Lenoir, D. Jérôme, P. Batail, *Phys. Rev. Lett.* **1995**, *75*, 4122, and references cited therein.
[9] H. E. Katz, M. L. Schilling, C. E. D. Chidsey, T. M. Putvinski, R. S. Hutton, *Chem. Mater.* **1991**, *3*, 699.
[10] a) M. Fourmigué, P. Batail, *Bull. Soc. Chim. Fr.* **1992**, *129*, 29; b) M. Fourmigué, Y.-S. Huang, *Organometallics* **1993**, *12*, 797; c) A. Dolbecq, M. Fourmigué, P. Batail, C. Coulon, *Chem. Mater.* **1994**, *6*, 1413.
[11] D. C. Green, *J. Org. Chem.* **1979**, *44*, 1476.
[12] S. Ganguly, J. T. Mague, D. M. Roundhill, *Inorg. Chem.* **1992**, *31*, 3500; C. E. McKenna, M. T. Higa, N. H. Cheung, M.-C. McKenna, *Tetrahedron Lett.* **1977**, *2*, 155; H. E. Katz, M. L. Schilling, *J. Org. Chem.* **1991**, *56*, 5318.
[13] J. C. Bonner, M. E. Fisher, *Phys. Rev. A* **1964**, *135*, 640; J. B. Torrance, Y. Tomkiewicz, B. D. Silverman, *Phys. Rev. B* **1977**, *15*, 4738.
[14] It is interesting to note that the latter compound can be regarded as a self-doped Bechgaard salt in which the covalently linked phosphonate anion acts as the discrete counteranion in the traditional $(TMTTF)_2X$ series. We are currently attempting to grow single crystals of this very interesting compound.
[15] a) M. Giffard, P. Alonso, J. Garin, A. Gorgues, T. P. Nguyen, P. Richomme, A. Robert, J. Roncali, S. Uriel, *Adv. Mater.* **1994**, *6*, 298; b) this is also consistent with our observations that the methanol hydrolysis of **3** under strictly anaerobic conditions (sealed evacuated tube) does not produce the black paramagnetic compound **5** but an extremely air-sensitive orange product instead.
[16] P. Lesfauries, P. Rumpf, *C. R. Acad. Sci.* **1949**, *228*, 1018; H. H. Jaffé, L. D. Freedman, G. O. Doak, *J. Am. Chem. Soc.* **1953**, *75*, 2209.
[17] K. H. Janzon, H. Schäfer, A. Weiss, *Z. Anorg. Allg. Chem.* **1970**, *372*, 87–99; see also A. F. Wells, *Structural Inorganic Chemistry*, 5th ed., Clarendon, Oxford, **1984**, p. 990.
[18] D. Venkataraman, S. Lee, J. Zhang, J. S. Moore, *Nature* **1994**, *371*, 591.
[19] S. Oliver, A. Kuperman, N. Coombs, A. Lough, G. A. Ozin, *Nature* **1995**, *378*, 47.
[20] See, for example: a) A. Pénicaud, P. Batail, P. Davidson, A.-M. Levelut, C. Coulon, C. Perrin, *Chem. Mater.* **1990**, *2*, 117; b) C. Livage, M. Fourmigué, P. Batail, E. Canadell, C. Coulon, *Bull. Soc. Chim. Fr.* **1993**, *130*, 761.
[21] *The Structural Chemistry of Phosphorus* (Ed.: D. E. C. Corbridge), Elsevier, New York, **1974**, ch. 9.
[22] Y. N. Kreitsberga, O. Y. Neiland, *J. Org. Chem. USSR* **1987**, 2131, English translation from *Zh. Org. Khim.* **1986**, *22*, 2372.
[23] A. Dolbecq, M. Fourmigué, P. Batail, *Bull. Soc. Chim. Fr.* **1996**, *133*, 83.
[24] E. G. Hutchinson, A. L. Morris, J. M. Thornton in *Structure Correlations, Vol. 2* (Eds.: H.-B. Bürgi, J. D. Dunitz), VCH, Weinheim, **1994**, pp. 635–667; see also T. E. Creighton, *Proteins, Structures and Molecular Properties*, 2nd ed., Freeman, New York, **1993**, p. 217.
[25] G. A. Jeffrey, W. Saenger, in *Hydrogen Bonding in Biological Structures*, Springer, Berlin, **1991**.
[26] Conventionally, when the highest occupied molecular orbital (HOMO) of a molecule is filled with just one electron it is referred to as SOMO (singly occupied molecular orbital). However, in order to facilitate the comparison of **7** with other π-donors of the TTF family we still refer to it as HOMO.
[27] a) M.-H. Whangbo, J. M. Williams, P. C. W. Leung, M. A. Beno, T. J. Emge, H. H. Wang, *Inorg. Chem.* **1985**, *24*, 3500; b) J. M. Williams, H. H. Wang, T. J. Emge, U. Geiser, M. A. Beno, P. C. W. Leung, K. D. Carlson, R. Thorn, A. J. Schultz, *Prog. Inorg. Chem.* **1987**, *35*, 51. Since overlap is explicitly included in extended Hückel calculations, these interaction energies should not be confused with the conventional transfer integrals. Although the two quantities are obviously related and have the same physical meaning, the absolute values of the interaction energies are somewhat larger than those of the transfer integrals.
[28] The values reported in Table 2 were calculated on the basis of the β-$(ET)_2I_3$ crystal structure reported in R. P. Shibaeva, V. F. Kaminskii, V. K. Bel'skii, *Sov. Phys. Crystallogr.* **1984**, *29*, 638.
[29] M.-H. Whangbo, J. M. Williams, P. C. W. Leung, M. A. Beno, T. J. Emge, H. H. Wang, K. D. Carlson, G. W. Crabtree, *J. Am. Chem. Soc.* **1985**, *107*, 5815; M.-L. Doublet, L. F. Veiros, E. Canadell, unpublished results.
[30] a) C. D. Bryan, A. W. Cordes, R. M. Fleming, N. A. George, S. H. Glarum, R. C. Haddon, R. T. Oakley, T. T. M. Palstra, A. S. Perel, L. F. Schneemeyer, J. V. Waszczak, *Nature* **1993**, *365*, 821; b) A. W. Cordes, R. C. Haddon, R. T. Oakley, *Adv. Mater.* **1994**, *6*, 798; c) C. D. Bryan, A. W. Cordes, R. M. Fleming, N. A. George, S. H. Glarum, R. C. Haddon, C. D. MacKinnon, R. T. Oakley, T. T. M. Palstra, A. S. Perel, *J. Am. Chem. Soc.* **1995**, *117*, 6880; d) C. D. Bryan, A. W. Cordes, J. D. Goddard, R. C. Haddon, R. G. Hicks, C. D. MacKinnon, R. C. Mawhinney, R. T. Oakley, T. T. M. Palstra, A. S. Perel, *ibid.* **1996**, *118*, 330.
[31] A. Guirauden, I. Johannsen, P. Batail, C. Coulon, *Inorg. Chem.* **1993**, *32*, 2446.
[32] Z. G. Soos, *J. Chem. Phys.* **1967**, *46*, 4284; D. B. Chesnut, W. D. Phillips, *ibid.* **1961**, *35*, 1002.
[33] D. Gundel, H. Sixl, R. M. Metzger, N. E. Heimer, R. H. Harms, H. J. Keller, D. Nöthe, D. Wehe, *J. Chem. Phys.* **1982**, *77*, 6203; J. C. Bailey, D. B. Chesnut, *ibid.* **1969**, *51*, 5118.
[34] S. R. Hall, H. D. Flack, J. M. Stewart, *XTAL 3.2 Reference Manual*; Universities of Western Australia, Geneva, and Maryland, **1992**.
[35] Crystallographic data (excluding structure factors) for the structures reported in this paper have been deposited with the Cambridge Crystallographic Data Centre as supplementary publication no. CCDC-1220-22. Copies of the data can be obtained free of charge on application to the Director, CCDC, 12 Union Road, Cambridge CB21EZ, UK (fax: int. code +(1223)336-033; e-mail: teched@chemcrys.cam.ac.uk).
[36] M.-H. Whangbo, R. Hoffmann, *J. Am. Chem. Soc.* **1978**, *100*, 6093.
[37] J. Ammeter, H.-B. Bürgi, J. Thibeault, R. Hoffmann, *J. Am. Chem. Soc.* **1978**, *100*, 3686.

0947-6539/96/0210-1282 $ 15.00+.25/0